ELSEVIER

Journal of Structural Geology 28 (2006) 519–535

JOURNAL OF STRUCTURAL GEOLOGY

www.elsevier.com/locate/jsg

Style and sequence of deformation during extensional fault-propagation folding: examples from the Hammam Faraun and El-Qaa fault blocks, Suez Rift, Egypt

C.A.L. Jackson *, R.L. Gawthorpe, I.R. Sharp [1]

Basin and Stratigraphic Studies Group, School of Earth, Atmospheric and Environmental Sciences, University of Manchester, Oxford Road, Manchester M13 9PL, UK

Received 9 January 2005; received in revised form 17 November 2005; accepted 24 November 2005

Abstract

Kilometre-scale fault-parallel folds are identified adjacent to normal faults in the Oligo-Miocene Suez Rift, Egypt and are interpreted to have formed in response to fault-propagation folding above upward propagating blind faults. The geometry, scale and distribution of secondary structures within the folds and their cross-cutting relationships with the master faults allow the style and sequence of deformation during fault-propagation folding to be established and suggest that during the initial stages of folding, the proto-footwall underwent extension which was accommodated by layer-parallel slip in encasing mudstone horizons and linked normal faulting and block rotation in carbonate and sandstone units. The proto-hanging wall also contains dominantly extensional normal faults although locally, where the master fault had a convex-into-the-footwall map-view trace, reverse faulting and fracturing occurred. Secondary structures adjacent to the master fault were not all active simultaneously, but initiated and died at different stages during the evolution of the fault-propagation fold. The results of this study confirm many key predictions of numerical and physical analogue models but also highlight several important controls on the evolution of fault propagation folds in extensional settings which existing models cannot capture, such as the influence of the map-view trace of the propagating fault and lateral variations in cover stratigraphy lithology and strength on the style and magnitude of secondary deformation.

Keywords: Fault-propagation folding; Normal faulting; Layer-parallel slip; Extensional basins; Suez Rift

1. Introduction

Fault-propagation folding is an important process during the early stages of fault growth in extensional settings as demonstrated by several field studies (e.g. Sterns, 1978; Schlische, 1995; Janecke et al., 1998; Maurin and Niviere, 2000; Sharp et al., 2000a; Khalil and McClay, 2002; Willsey et al., 2002). The geometry and evolution of fault-propagation folds have also been investigated in the subsurface using three-dimensional seismic data (e.g. Withjack et al., 1989; Pascoe et al., 1999; Corfield and Sharp, 2000; Withjack and Callaway, 2000). Based on these field and subsurface studies, numerical and physical analogue models have been developed to investigate the controls on the overall geometric evolution of fault-propagation folds (e.g. Vendeville, 1987; Withjack et al., 1990; Mitra and Islam, 1994; Patton and Fletcher, 1995; Allmendinger, 1998; Hardy and McClay, 1999; Withjack and Callaway, 2000; Finch et al., 2004; Patton, 2004). These models provide important insights into the manner in which deformation is accommodated within the evolving fold and suggest that a combination of normal and reverse faulting, folding and bedding-parallel slip are important deformation mechanisms (Fig. 1A and B). Although recent numerical models can directly model structures accommodating faulting and folding (cf. Finch et al., 2004), the majority of such models typically only predict bulk strain distribution through time and thus the distribution and orientation of structures accommodating this strain must be inferred (e.g. Erslev, 1991; Patton and Fletcher, 1995; Allmendinger, 1998; Hardy and McClay, 1999). Physical analogue models, although able to replicate physically some of the small-scale structures, are typically constructed on the centimetre-scale; thus it is difficult to observe how secondary deformation mechanisms are related (Vendeville, 1987;

* Corresponding author. Present and correspondence address: Department of Earth Sciences and Engineering, Prince Consort Road, Imperial College, London SW7 2BP, UK. Tel.: +44 7903 033298; fax: +44 207 5947444.
E-mail address: c.jackson@imperial.ac.uk (C.A.L. Jackson).
[1] Present address: Norsk Hydro Research Centre, Sandsliveien 90, 5020, Bergen, Norway.

0191-8141/$ - see front matter © 2006 Elsevier Ltd. All rights reserved.
doi:10.1016/j.jsg.2005.11.009

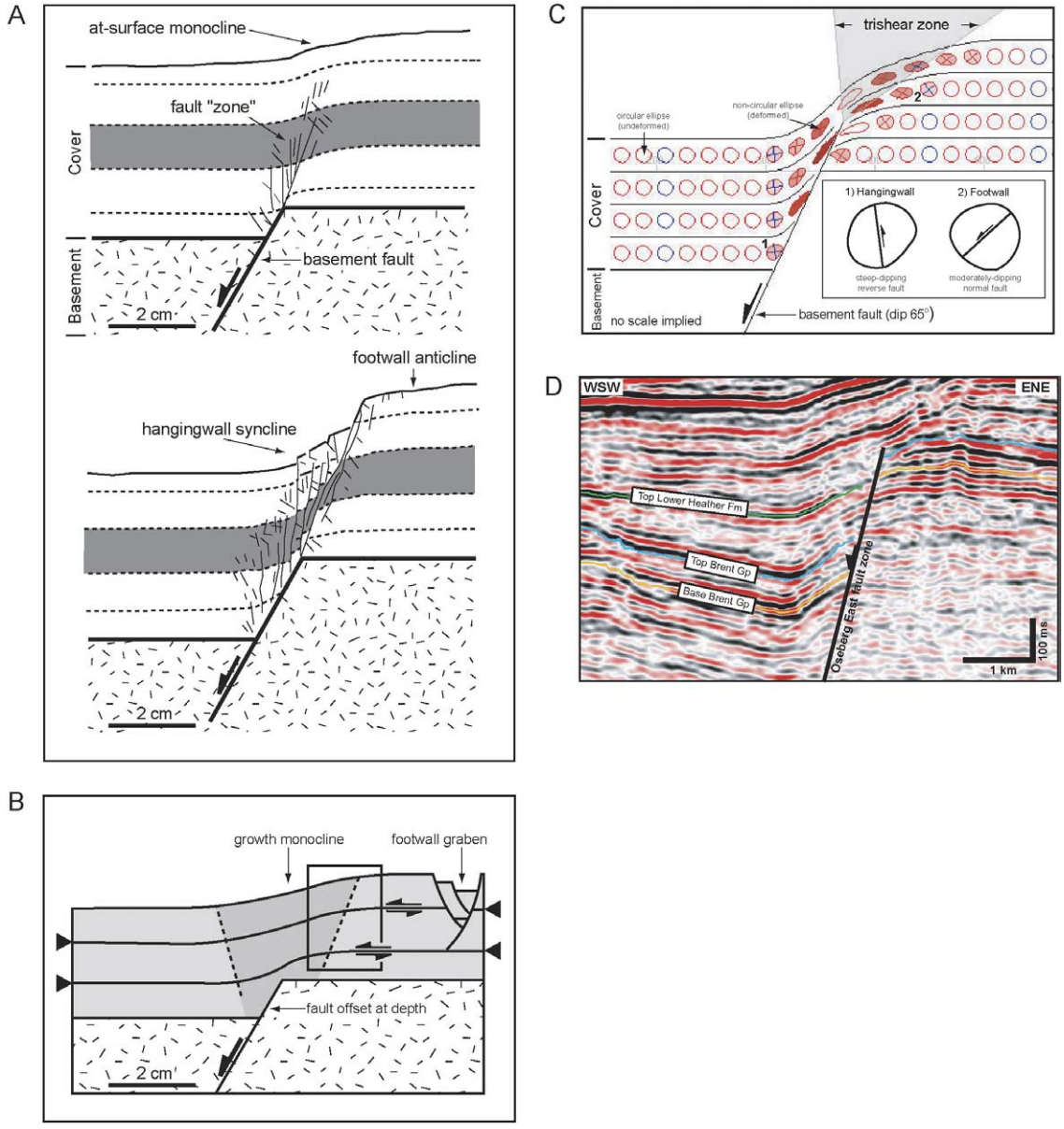

Fig. 1. (A) Cross-section from a physical analogue model of Withjack et al. (1990) illustrating the development of a fault-propagation fold above an upwardly-propagating fault-tip. Note distribution and orientation of secondary structures. (B) Summary diagram of physical analogue model by Withjack et al. (1990) illustrating the influence of layer-parallel detachments (black arrows) in the cover stratigraphy on the evolution of an extensional fault-propagation fold. (C) 'Trishear' numerical model of an extensional fault-propagation fold (Allmendinger, 1998). Shaded spheres are deformed during folding and lines within spheres are lines-of-no-finite-elongation (LNFE) used to infer the orientation of secondary faults and fractures. Inset shows attitude of secondary structures in the footwall and hanging wall inferred from LNFE. (D) Seismic section across a breached fault-propagation fold adjacent to the Oseberg East fault, North Viking Graben.

Withjack et al., 1990; Mitra and Islam, 1994; Withjack and Callaway, 2000). A similar resolution problem affects subsurface studies due to the typically low resolution of the seismic data used (Withjack et al., 1989; Pascoe et al., 1999; Corfield and Sharp, 2000).

Although outcrop analysis allows observations to be made at a scale intermediate between modelling and subsurface studies, relatively few field studies have specifically investigated the exact manner in which deformation is accommodated during fault-propagation folding (Gross et al., 1997; Keller and Lynch, 2000; Willsey et al., 2002; Grant and Kattenhorn, 2004; Fodor et al., 2005). The majority of these field studies have focused on relatively small areas adjacent to only one fault zone within the respective study areas, thus it is unclear if models derived from these studies are applicable to fault-propagation folds in other settings. In this paper we document the manner in which deformation is accommodated during fault-propagation folding through structural analysis of six normal fault zones (herein termed master faults) in the central part of the Oligo-Miocene Suez Rift, Egypt. To achieve this we describe the overall structural style of the fault-related folds, before focusing on the geometry, orientation, scale and distribution of secondary structures adjacent to the master faults. Cross-cutting relationships between the master faults and secondary structures,

and thickness variations in adjacent syn-rift units where preserved are then used to establish the temporal evolution of secondary deformation associated with fault-propagation folding. A model is proposed for the evolution of fault-propagation folds in extensional settings which, although based on observations from the Suez Rift, may be equally applicable to other extensional settings. This model stresses that many of the deformation processes are kinematically-linked and confirms many of the key predictions of existing numerical and physical analogue models.

The Suez Rift is an excellent location in which to conduct this study, as a combination of regional uplift achieved without compression, desert-style environment and recent fluvial incision results in exceptional 3D exposures of all the studied faults and associated folds. Furthermore, the absence of post-rift compression means that the original geometrical relationship between all of the rift-related structures is preserved. Crucially, and in contrast to other studies, this allows us to: (1) compare the style and sequence of deformation between several fault zones within the same tectonic setting, and (2) study deformation along-strike of the faults over significantly longer length-scales (i.e. 10–50 km) than previously considered.

2. Geological setting

The Suez Rift forms the NW–SE-trending arm of the Cenozoic Red Sea rift system that formed in response to Late Oligocene–Early Miocene rifting of the African and Arabian plates (Garfunkel and Bartov, 1977; Colletta et al., 1988; Lyberis, 1988; Patton et al., 1994). The rift is 300 km long and up to 80 km wide and is delineated on both margins by large-scale NW–SE-striking normal fault zones that define half-grabens. The study area is located in the central part of the rift within the Hammam Faraun and El-Qaa fault blocks, two 40-km-long by 25-km-wide fault-bounded half-grabens tilted gently (10–20°) towards the NE (Moustafa and Abdeen, 1992) (Fig. 2A). Both fault blocks are bounded by large displacement (2–5 km), down-to-the-southwest normal faults: the Eastern Boundary Fault Belt (EBFB) and Coastal Fault Belt (CFB) to the east and west, respectively (fault terminology after Sharp et al. (2000b)). This study focuses on the Hammam Faraun, Baba-Markha and Abu Zenima fault zones located along the northern part of the CFB, and the Thal, Baba-Sidri and Hadahid fault zones located along the EBFB (Fig. 2A and B). Seismic data from the Gulf of Suez and the Baba-Markha plain (Fig. 2) indicate that the Hammam Faraun and Baba-Markha fault zones dip steeply (60–70°), are planar down to at least 3 km and do not appear to change in dip as they approach the present-day free surface (see fig. 8 in Gawthorpe et al., 2003). Slickenside data from all the studied fault zones indicate dominantly dip-slip movement, although data from the Baba-Markha fault zone suggests this structure experienced a minor component of sinistral strike-slip movement probably due to this fault being orientated E–W and therefore at a high-angle to the overall NW–SE rift trend (Moustafa and Abdeen, 1992; Gilpin, 1998).

The pre-rift stratigraphy of the study area can be divided into two megasequences which have a combined thickness of ca. 850 m (Fig. 3) (Robson, 1971; Moustafa, 1987; Sharp et al., 2000a). Megasequence One consists of the predominantly non-marine Nubian sandstones (Cambrian–Lower Cretaceous) which overlie Precambrian metamorphic basement. Megasequence Two comprises a mixed carbonate–clastic succession (Raha, Wata, Matulla, Duwi and Sudr Formations) of Cretaceous age and an overlying mixed carbonate–mudstone sequence (Esna, Thebes, Darat and Tanka Formations) of early Tertiary age. Of particular importance to the structural evolution of the area is the mechanical contrast represented by the transition between the mudstone-dominated stratigraphic intervals, in particular the Esna, Duwi and Wata Formations, and the rest of the carbonate and sandstone-dominated stratigraphy (Fig. 3).

Late Oligocene–Early Miocene non-marine (Abu Zenima Formation—24–21.5 Ma) and marginal marine (Nukhul Formation—21.5–19.7 Ma) clastics represent the earliest syn-rift units and unconformably overlie the pre-rift strata to form the lower part of Megasequence Three (Fig. 3) (Patton et al., 1994; Bentham et al., 1996; Krebs et al., 1997; Montenat et al., 1998; Carr et al., 2003). These units were deposited during the rift-initiation stage when deformation was distributed across the fault block on numerous short (1–4 km), low-displacement (< 1 km), intra-block faults (Sharp et al., 2000b; Gawthorpe et al., 2003). The overlying, open marine Lower Rudeis Formation (19.7–15.5 Ma) was deposited during the rift-climax stage at which time many of the intra-block faults became inactive and fault activity was progressively localised onto the master EBFB and CFB some 6–7 My after the start of rifting (Patton et al., 1994; Sharp et al., 2000b; Gawthorpe et al., 2003; Jackson et al., 2006).

3. Structural style of the master faults and related folds

3.1. East Boundary Fault Belt (EBFB)

Detailed structural mapping along the Thal and Baba-Sidri fault zones of the EBFB indicates the development of fault-parallel footwall anticlines and hanging wall synclines adjacent to the master faults (Sharp et al., 2000a). The footwall anticlines are 2–3 km wide, and are defined by a change from gentle (<10°) stratal dips away from the fault more than 3 km into the footwall, to moderate and steep (17–54°) stratal dips towards the fault in the immediate footwall of the master fault zone (cross-section A–A′; Figs. 2B and 4). Along the Baba-Sidri fault zone the hanging wall syncline is up to 4 km wide, being bound on its western margin by the Nezzazat fault zone (Fig. 4), whereas the syncline in the hanging wall of the Thal fault zone is 16–20 km wide and defines the full width of the Hammam Faraun half-graben (cross-section A–A′; Fig. 2B). In both cases the hanging wall synclines are strongly asymmetric, with a moderately to very steeply (20–80° and locally overturned) south-westwards dipping limb adjacent to the master fault and a more gently-dipping (20–30°) eastwards-dipping opposing limb (Fig. 4). The fault-parallel hanging

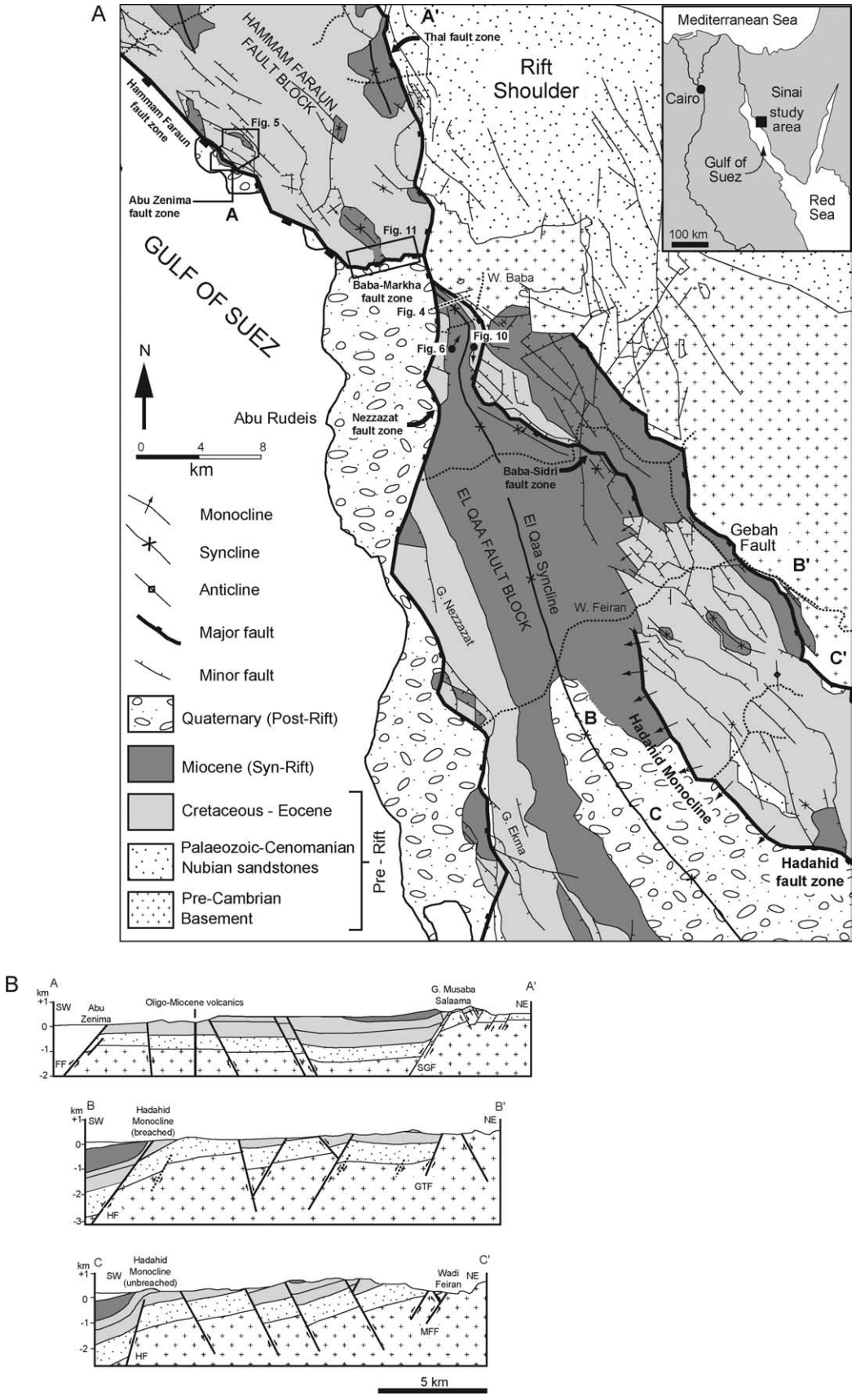

Fig. 2. (A) Simplified geological map of the Hammam Faraun and El Qaa fault blocks, western Sinai. The main faults and localities discussed in the text are marked. Modified after Robson (1971), Garfunkel and Bartov (1977), Moustafa (1993) and Sharp et al. (2000a). The location of Figures 2B 4, 5, 6, 10 and 11 are marked.

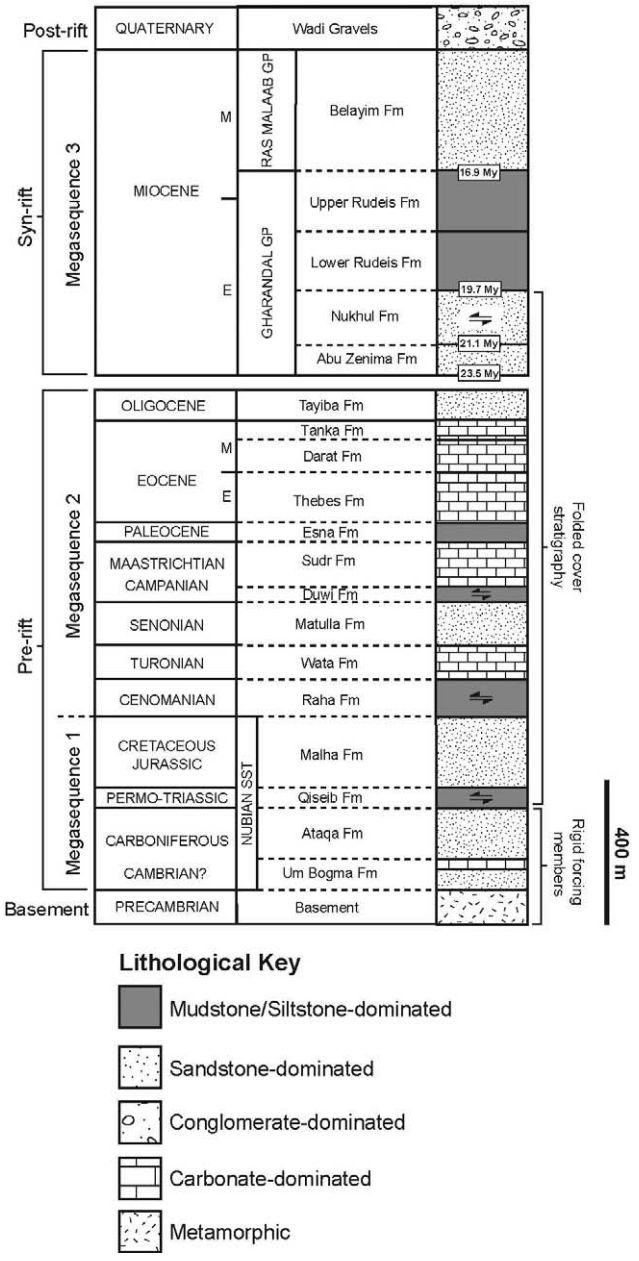

Fig. 3. Composite stratigraphic section of the Hammam Faraun and El-Qaa fault blocks, western Sinai modified from Moustafa (1987). Mudstone-dominated units which represent major layer-parallel slip horizons are indicated by opposing black arrows. Ages of key stratigraphic surfaces bounding early syn-rift units are also indicated (Jackson et al., 2002).

wall syncline can be mapped for >75 km along strike of the EBFB although its along-strike trace is offset by the younger Baba-Markha fault zone (Fig. 2A).

Structural transects across the southern end of the Hadahid fault zone (Fig. 2) where the fault has 1 km displacement reveal a similar geometry to that observed adjacent to the Baba-Sidri and Thal fault zones, with a fault-parallel anticline and an asymmetric, fault-parallel syncline developed in the footwall and hanging wall of the fault, respectively (cross-section B–B′; Fig. 2B). North of this location the Hadahid fault zone loses displacement and the footwall–hanging wall fold pair is replaced at surface by a 4-km-wide, SW-facing monocline located above the buried fault tip (cross-section C–C′; Fig. 2B). A similar along-strike transition from a surface-breaking fault zone to a basinward-facing monocline above a blind fault tip has also been documented for several of the intra-block faults within the Hammam Faraun fault block (Jackson et al., 2002; Carr et al., 2003; Gawthorpe et al., 2003) (Fig. 2).

3.2. Coastal Fault Belt (CFB)

Although the hanging wall to the CFB is buried under thick deposits of Quaternary gravels onshore (see Fig. 2A and B) and not clearly resolved on seismic data offshore, the footwall is exceptionally well exposed and is characterised by a fault-parallel anticline up to 3 km wide which is defined by a steepening of bedding with increasing proximity to the fault zone (Fig. 5). The fault-parallel anticline can be mapped for a total of 22 km along-strike of the CFB, trending NW–SE and E–W adjacent to the Hammam Faraun and Baba-Markha fault zones, respectively. The along-strike exposure of the fold is controlled either by younger faults that dissect the structures (e.g. Baba-Sidri fault zone at eastern end of the Baba-Markha fault zone; Fig. 2A) or the limit of exposure (e.g. northern end of the Hammam Faraun fault zone where the fold is inferred to run offshore; Fig. 2A).

4. Evolution of the master faults and related folds

Fault-parallel footwall anticlines and hanging wall synclines developed adjacent to the master faults have previously been ascribed to variations in fault dip with depth (Colletta and Moretti, 1985), drag adjacent to the master faults (Moustafa, 1987), or post-rift, gravity-driven crustal shortening (Knott et al., 1995; Knott, 2001). When considering these mechanisms it is observed that although variations in master fault dip with depth are observed, this dip variability (commonly <10°) is considered insufficient to be responsible for the scale of folds observed in the Suez Rift. Furthermore, this model does not account for the fault-parallel anticlines developed in the footwall to the master fault, thus variations in fault dip with depth are unlikely to be the main mechanism responsible for fault-related folding in the study area. The scale of the folding adjacent to the faults is on the kilometre-scale, thus is an order of magnitude greater than folding associated with frictional drag, which is typically on the 10–100's of metres scale. Finally, in the hanging walls of the Thal and Baba-Sidri fault zones, syn-rift stratal units thin and onlap towards

(B) Cross-sections across (A–A′) the Hammam Faraun fault zone block and (B–B′ and C–C′) the Hadahid fault zone of the El-Qaa fault block. Note the faulted monocline configuration associated with the Hadahid fault zones which passes laterally into an unbreached monocline. See Figure 2A for location of cross sections. After Garfunkel and Bartov (1977) and Moustafa (1993).

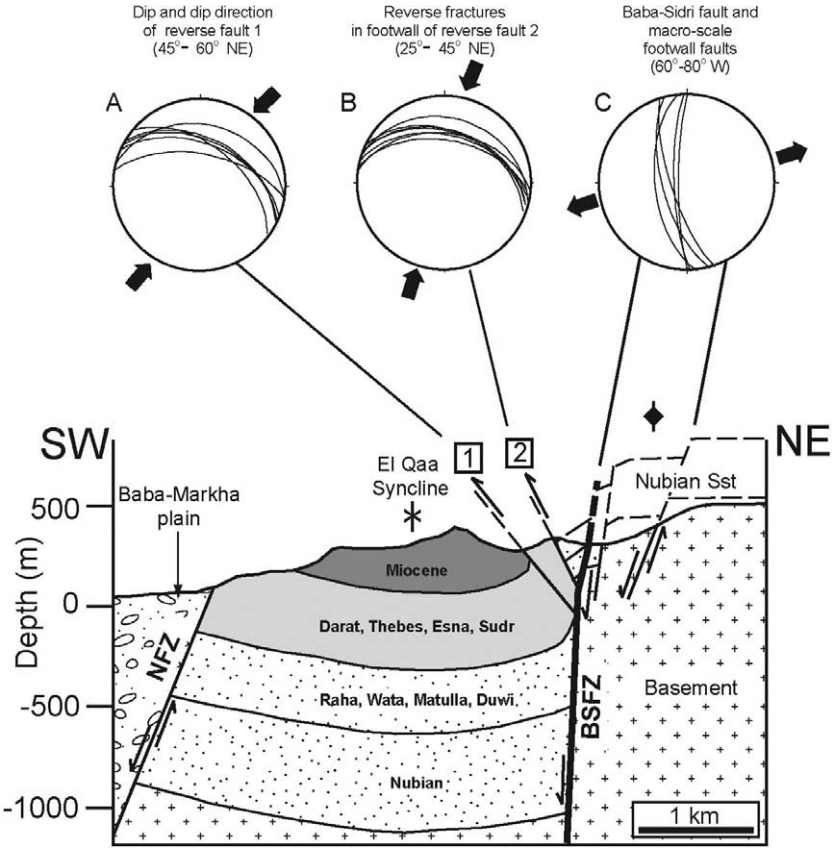

Fig. 4. Simplified cross-section across the northern end of the Baba-Sidri fault zone (BSFZ) where the fault strikes NW–SE. See Fig. 2A for location of cross-section. Note the faulted monocline configuration associated with the master fault and secondary macro-scale normal and reverse faults developed in the footwall and hanging wall, respectively. Lower hemisphere stereonet projections of plane dip and dip direction are provided to illustrate the orientation and attitude of (A) macro-scale reverse fault 1, (B) meso-scale reverse faults/fractures associated with fault 2, and (C) the Baba-Sidri fault zone and associated macro-scale footwall faults. Black arrows adjacent to the stereonets indicate the dominate strain inferred from the secondary structures. NFZ = Nezzazat fault zone.

faults on the flanks of the hanging wall syncline (Gawthorpe et al., 1997, 2003; Gupta et al., 1999; Sharp et al., 2000a; Young et al., 2002), clearly indicating that the hanging wall folds (and presumably their footwall equivalents) formed synchronous with the main period of extension and are not post-rift features (cf. Knott et al., 1995; Knott, 2001).

A key observation when interpreting the origin of the fault-parallel folds is that along several of the master and intra-block faults, the fault-parallel folds can be traced laterally, parallel to fault strike, into unbreached monoclines at the fault tips. Based on these observations, and following previous field studies along the Thal (Young et al., 2002) and Baba-Sidri fault zones (Gawthorpe et al., 1997; Gupta et al., 1999; Sharp et al., 2000a) the fault-parallel folds are interpreted as breached monoclines that originally formed as a result of fault-propagation folding above upward-propagating blind faults (Fig. 1A). The same mechanism has also been interpreted to be responsible for the development of kilometre-scale folds adjacent to large normal faults in other parts of the Suez Rift (Patton, 1984; Khalil and McClay, 2002).

Adjacent to the master faults a variety of secondary structures are observed. In the following section, the geometry, scale and distribution of these structures adjacent to the master faults are described. Particular emphasis is placed on the spatial relationship between deformation mechanism and lithology, cross-cutting relationships between the secondary structures and master faults, and the architecture of syn-rift units adjacent to the secondary structures.

5. Structural style of secondary structures

5.1. Macro-scale deformation

The term macro-scale deformation is used to define structures including and associated with faults >400 m in length and with >50 m displacement. We begin by describing macro-scale deformation in the footwalls of the master faults described above, before moving on to describe deformation in their hanging walls.

5.1.1. Footwall deformation

In the footwall to the Hammam Faraun fault zone, within the SW-dipping limb of the fault-parallel footwall anticline, a series of NW–SE-striking, steeply-dipping (60–70°) faults up to 5 km long and with up to 400 m displacement are developed. These faults splay and link up along-strike and show pronounced lateral variations in displacement. Footwall anticlines and

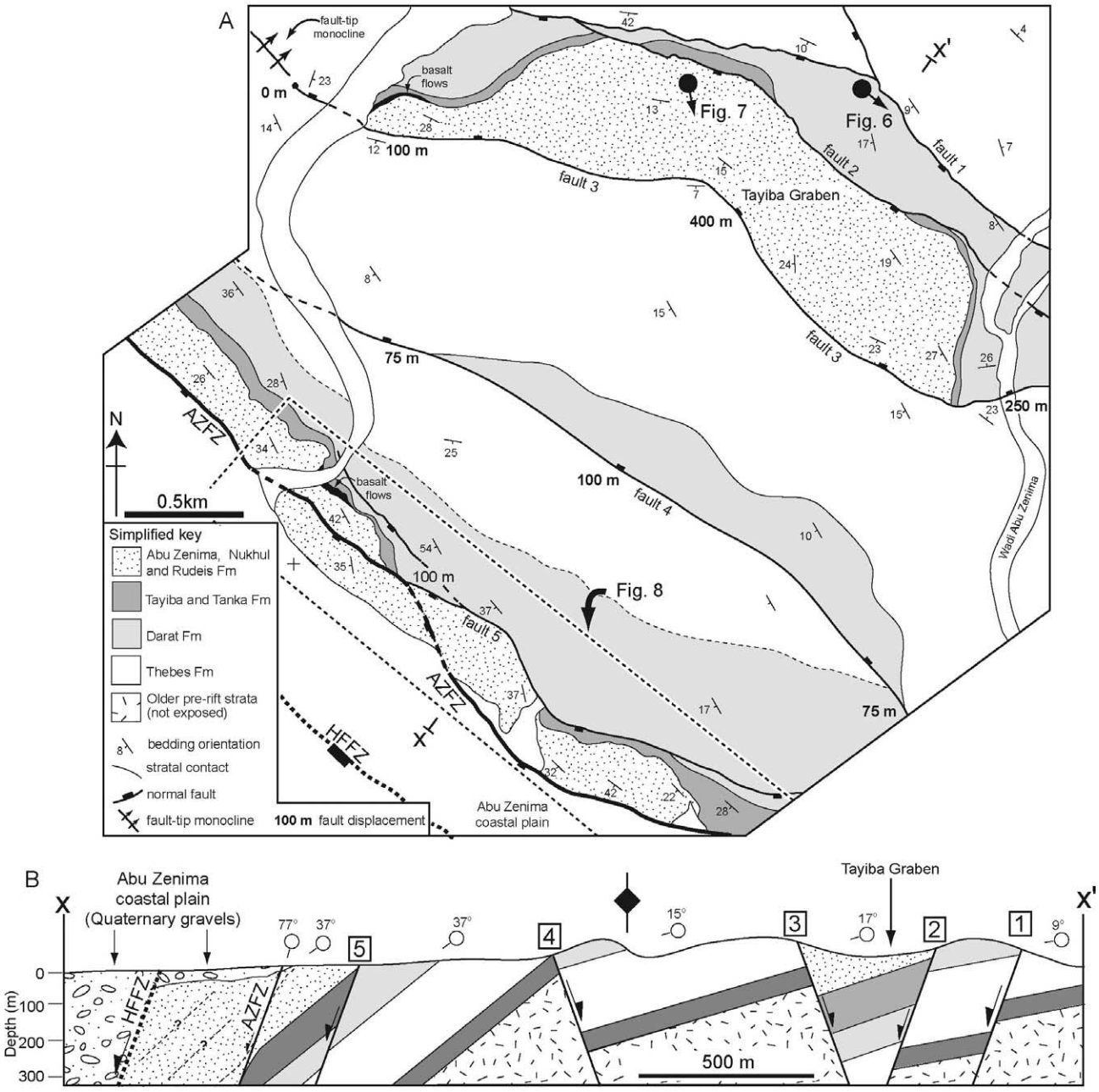

Fig. 5. (A) Geological map illustrating the structure of the footwall to the Hammam Faraun fault zone. See Fig. 2A for location. Faults 1–5 refer to macro-scale faults discussed in the text and indicated on (B). The locations of Figs. 7 and 8 are marked. (B) Cross-section illustrating the fault-parallel footwall anticline associated with the Hammam Faraun fault zone. The fault-parallel anticline is deformed by a series of macro-scale normal faults. See (A) for location of section.

hanging wall synclines are developed adjacent to the macro-scale faults and can be traced laterally, parallel to fault strike, into unbreached monoclines (e.g. NW end of fault 3; Fig. 5A and B). These macro-scale faults bound a series of horsts and grabens up to 3 km long by 750 m wide, one of which contains a 150-m thick succession of early syn-rift sediments (the Tayiba half-graben; Fig. 5). Within this depocentre, the rift-initiation Abu Zenima and Nukhul Formations have tabular geometries and display no systematic thickness variations with respect to the graben-bounding faults, whereas the lower part of the overlying Lower Rudeis Formation has a distinct wedge-shaped geometry and thickens into the hanging wall of the fault bounding the SW margin of the graben (Fig. 7). Based on the stratigraphic ages of these units (see Fig. 3), these observations indicate that the fault bounding the SW margin of the graben and probably the other macro-scale faults in the footwall of the Hammam Faraun fault zone, became active ca. 3.8 My after the initiation of rifting. The significance of this observation for the temporal relationship between the footwall faults, the master fault and associated fault-propagation fold is discussed further below.

Macro-scale footwall faults are also observed along the SW-dipping Thal, Baba-Sidri and Hadahid fault zones of the EBFB. The faults strike NW–SE parallel to and are restricted to

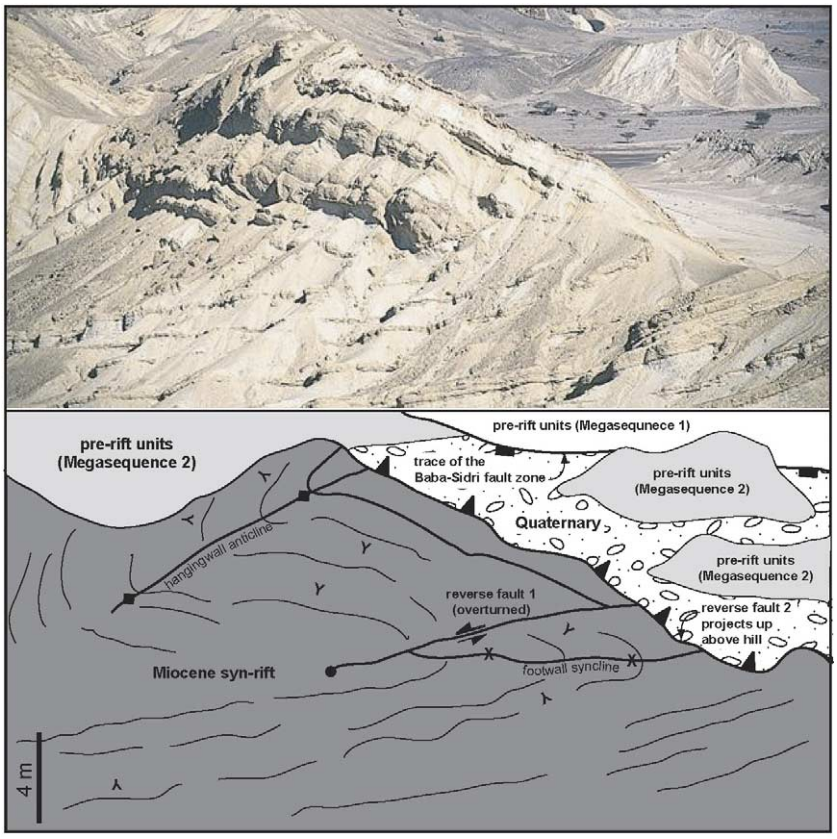

Fig. 6. (A) Photograph and (B) interpretative line drawing illustrating the development of macro-scale reverse faults in the hanging wall of the Baba-Sidri fault zone (BSFZ). Note that reverse 1 which tips out into the hanging wall is overturned in the footwall to the overlying reverse fault 2. Location of figure is shown in Fig. 2A.

the 1–3-km-wide zone in the footwall of the master faults (Figs. 2A and B and 4). The faults are either synthetic or antithetic to the master faults (stereonet C; Fig. 4), have 50–400 m displacement and display marked along-strike variations in displacement. With increasing proximity to the master faults, displacement on the normal faults increases, as does the amount of bedding tilt between them (cross-section A–A′; Figs. 2B and 4). Faults in the footwall of the Baba-Sidri fault zone are generally planar at the outcrop scale, although larger outcrops indicate that some of the macro-scale faults have a sigmoidal geometry in cross-section, dipping steeply ($>70°$) within and bounding rotated blocks of massive carbonate or sandstone units and tipping-out upwards and downwards into highly-sheared mudstone-dominated units interpreted as layer-parallel slip horizons (Sharp et al., 2000a).

5.1.2. Hanging wall deformation

Macro-scale deformation in the hanging walls of the master faults is dominated by steep-dipping (60–80°), moderate displacement (200–400 m) normal faults that trend parallel to the master faults and are up to 3 km in length. Such structures are particularly well-exposed along the Thal and Baba-Sidri fault zones of the EBFB. In these locations the faults are restricted to a 100–200 m zone in the hanging wall of the master faults and, where spaced <10 m, bound intensely deformed rider blocks of pre-rift strata of various ages within which bedding is steep ($>60°$). Mudstone-dominated units such as the Wata, Matulla and Esna Formations are attenuated or completely sheared-out, whereas brittle deformation such as fracturing and brecciation typifies massive carbonate and sandstone-dominated units such as the Thebes, Sudr and Raha Formations.

Although normal faulting dominates macro-scale hanging wall deformation, along the northern and central portions of the Baba-Sidri fault zone where the fault has a convex-into-the-footwall map-view trace, reverse faults that splay off the master fault and deform the steep limb of the fault-parallel hanging wall syncline are well-developed . The reverse faults have up to 100 m displacement and dip 20–60° towards the NE, with faults at structurally higher levels within the hanging wall usually dipping more steeply than underlying ones (Figs. 4 and 6).

5.2. Meso-scale deformation

The term meso-scale deformation is used to define structures including and associated with faults <100 m in length and with <50 m displacement. First we describe meso-scale deformation in the footwalls of the master faults, before moving on to describe deformation of a similar scale in their hanging walls.

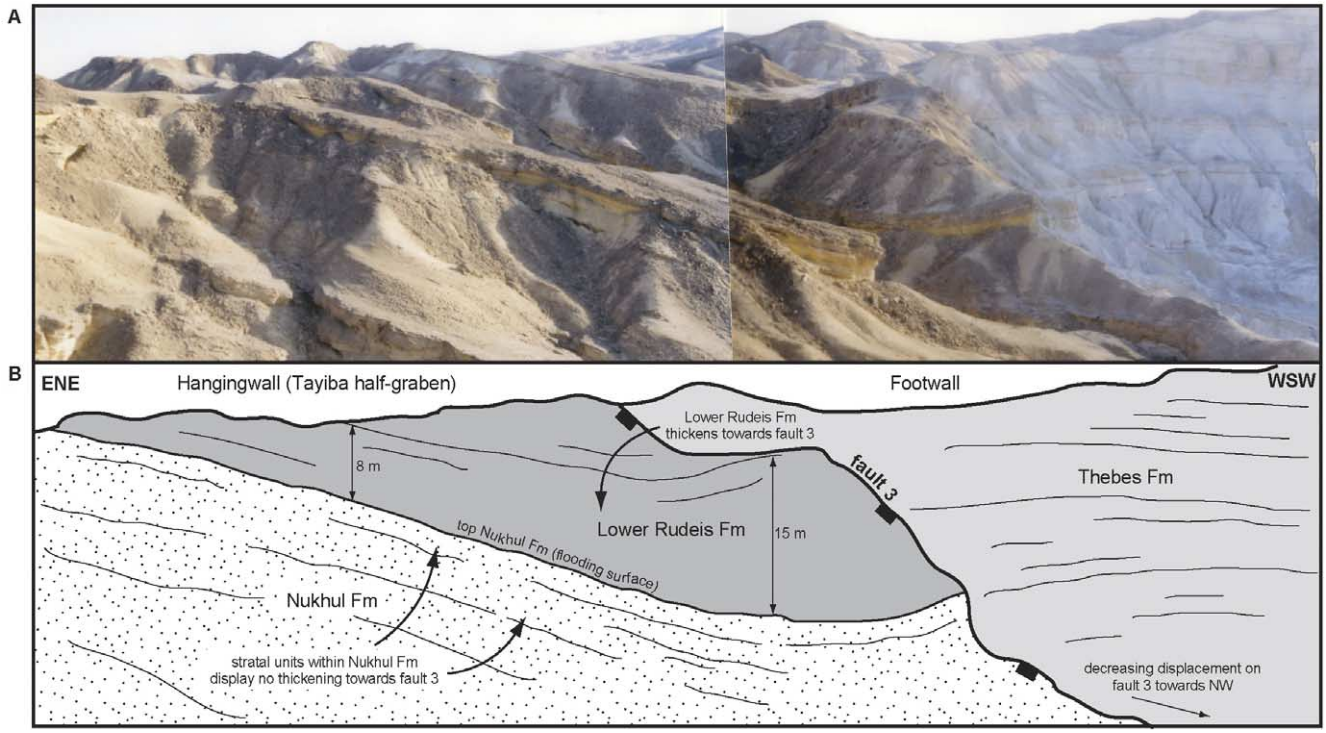

Fig. 7. (A) Field photograph and (B) interpretative line drawing illustrating thickness variations in early syn-rift units in the Tayiba half-graben developed in the footwall to the Hammam Faraun fault zone. The Nukhul Formation displays an overall tabular stratal geometry, whereas the overlying Rudeis Formation displays a pronounced wedge-shaped geometry that thickens into the hanging wall of fault 3 bounding the SW margin of the half-graben. See Fig. 5 for location of photograph.

5.2.1. Footwall deformation

Exposures in the footwalls of the Abu Zenima and Baba Sidri fault zones allow meso-scale footwall deformation to be characterised and indicate that layer-parallel slip horizons are well-developed, which manifest as highly sheared and attenuated mudstone horizons up to 1.75 m thick and are developed within pre- and syn-rift units of all ages at various levels within the footwall stratigraphy (Fig. 3). Normal faults are also common and are closely associated with the layer-parallel slip horizons. These faults are up to 100 m long, strike NW–SE to NNW–SSE and are synthetic (i.e. SW) or antithetic (i.e. NE) to the adjacent master fault zones (stereonets A–C; Fig. 8). Based on their cross-sectional geometry and degree of layer-confinement the meso-scale faults can be divided into three groups. The first group of faults are planar, steeply-dipping (up to 80°), have a maximum displacement of 15 m and typically strike oblique to and intersect with the master fault zone (Fig. 8). The second group comprise layer-unconfined normal faults with up to 2 m of displacement. These faults are listric to sigmoidal in cross-section, dip steeply (up to 80°) within carbonate and sandstone units and shallow upward and downward into underlying and overlying mudstone horizons, within which highly-sheared layer-parallel slip horizons are well-developed (Fig. 9A and B). The third group of faults are listric and have 20–30 cm of displacement. In contrast to the first two groups of meso-scale fault, these faults are layer-confined and cluster exclusively within highly sheared and attenuated mudstone-dominated units.

Meso-scale faults display marked variations in dip with increasing proximity to both the Abu Zenima and Baba-Sidri fault zones. Faults synthetic to the master faults which are located >250 m into the footwall dip 60–80° (stereonet pair A; Fig. 8). With increasing proximity to the master fault and with increasing bed rotation these faults increase in dip to $>80°$, ultimately being overturned where bedding is steep to overturned, thereby manifesting as steeply-dipping (70–80°) reverse faults (stereonet pairs B and C; Figs. 8 and 10). Faults antithetic to the master faults also display a marked variation in dip with increasing proximity to the master faults, manifesting as low-angle ($<5°$) reverse faults where bedding is steep to overturned (stereonet pair C; Figs. 8, 9C and 10). In the immediate footwall of the master fault zone, both synthetic and antithetic meso-scale footwall faults are truncated by the master fault, implying they formed prior to the master fault and before the monocline was breached (Figs. 9C and 10).

Meso-scale faults are also well developed in the footwall of the Baba-Markha fault zone, where there is marked vertical and lateral variability of stratigraphic units and hence lithologies. Along the eastern and western parts of the fault zone, carbonate and sandstone-dominated units of the pre-rift Wata, Matulla, Sudr, Thebes and Darat Formations form the footwall units, whereas heterolithic units of the early syn-rift Abu Zenima and Nukhul Formations are present along the centre of the fault zone (Fig. 11). Associated with these lateral variations in lithology are marked lateral variations in meso-scale deformation style and intensity. For example, along the central part of the Baba-Markha fault zone, where the Abu Zenima and Nukhul Formations form the footwall units, numerous low-displacement (<10 m), moderately to steeply (40–85°) dipping faults are present that strike parallel to and increase

in frequency towards the Baba-Markha fault zone (Fig. 11). The Nukhul Formation diverges into the hanging walls of the meso-scale faults suggesting these faults became active ca. 2.4 My after the initiation of rifting. Along the eastern and westernmost parts of the Baba-Markha fault zone within pre-rift carbonate and sandstone-dominated units, meso-scale faults are less well-developed but, where observed, they strike parallel to the Baba-Markha fault zone and have <1 m

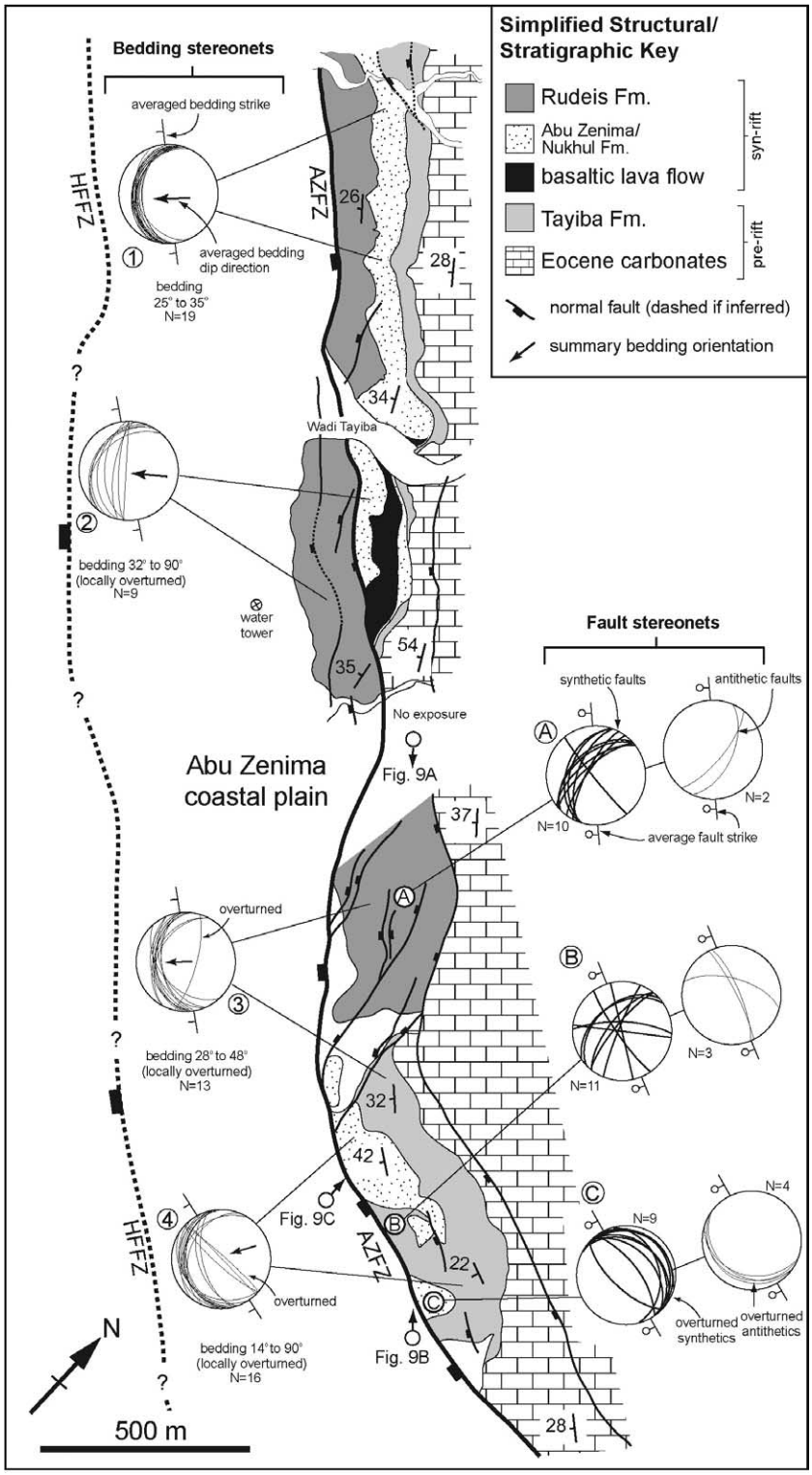

Fig. 8. Geological map of the footwall to the Hammam Faraun fault zone. See Fig. 5A for location. The locations of Fig. 9A–C are marked. The location and orientation of the Hammam Faraun fault zone is inferred from exposures of the fault zone north and south of the study area as mapped by Moustafa (1993). Lower hemisphere stereonet plots of plane orientation and plane dip illustrate the attitude of bedding (stereonets 1–4) and macro- and meso-scale normal faults (stereonet pairs A–C).

displacement (Fig. 11). Where larger (>5 m) displacement faults are observed they are considerably more complex than those identified along the central part of the Baba-Markha fault zone. For example, ca. 200 m into the footwall of the fault zone, a ramp–flat–ramp fault is developed in pre-rift units of the Matulla, Duwi and Sudr Formations (Fig. 12). The steeply-dipping ramp portions of the fault are located in the sandstone-dominated Matulla and carbonate-dominated Sudr Formations, with the intervening flat portion, which represents a major layer-parallel detachment, located within the mudstone-dominated Duwi Formation. Internally, the Duwi Formation is also intensely folded and highly attenuated with prominent thinning of the unit in the vicinity of the fault 'flat' (Fig. 12). Attenuation of the unit is associated with clusters of low-displacement (<1 m), layer-confined listric faults similar to the second group of meso-scale footwall faults described previously from the Abu Zenima and Baba-Sidri fault zones. Marked thickness variations are also observed in a 1-m-thick clay-rich interval at the top of the Duwi Formation, due to a series of low-displacement faults in the overlying Sudr Formation tipping-out downwards into this interval (Fig. 12).

5.2.2. Hanging wall deformation

Meso-scale hanging wall deformation is typically characterised by low-displacement (<10 m), synthetic and antithetic normal faults that strike parallel to the master fault. Along the northern and central portions of the Baba-Sidri fault zone where the fault is convex-into-the-footwall and macro-scale

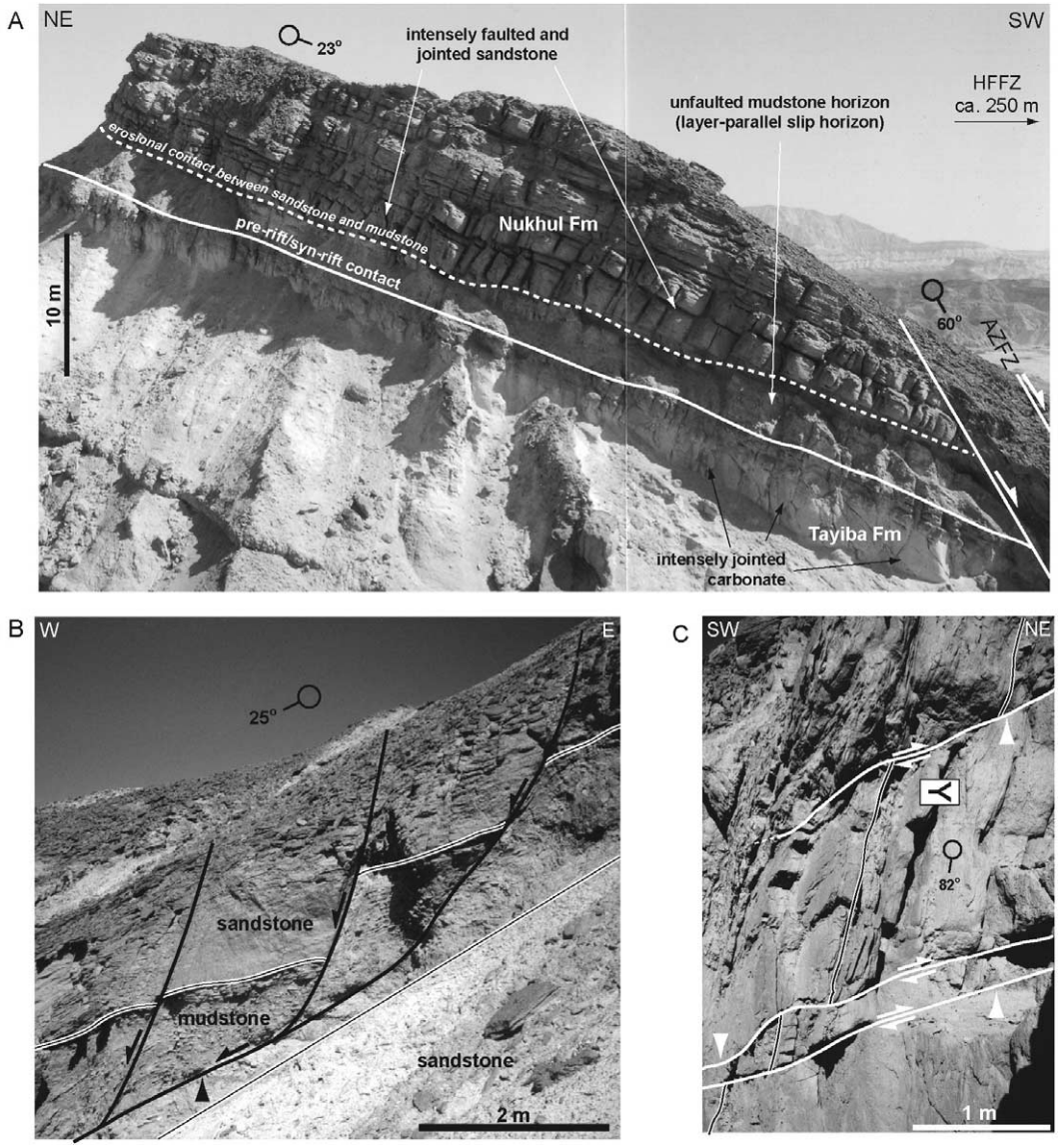

Fig. 9. Photographs illustrating the style of meso-scale faulting in the early syn-rift Nukhul Formation identified in the immediate footwall of the Abu Zenima fault zone. See Fig. 8 for location of photographs. (A) Pervasive faults and joints developed in tidal channel sandstones that detach downwards into a thick lagoonal mudstone horizon. Carbonates of the underlying Tayiba Formation are also intensely jointed. (B) Layer-unconfined listric faults that detach downwards onto a shared layer-parallel slip horizon (black arrow) located within a mudstone horizon. Note marked attenuation of the mudstone horizon. (C) Overturned meso-scale faults (white arrows) antithetic to the Abu Zenima fault zone now manifesting as low-angle reverse faults. Y indicates direction of stratigraphic-younging.

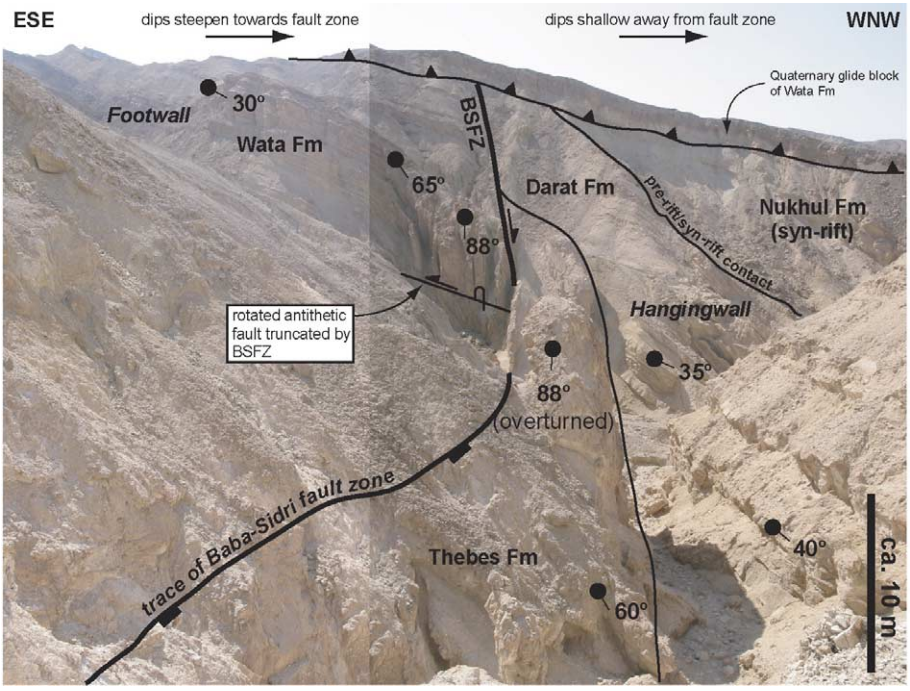

Fig. 10. (A) Annotated field photograph illustrating the breached monocline geometry developed adjacent to the master Baba-Sidri fault zone (BSFZ). Location is shown on Fig. 2A. Note the zone of very-steep to locally overturned bedding immediately adjacent to the fault and the antithetic meso-scale footwall fault which is overturned and truncated by the BSFZ.

reverse faults are observed, meso-scale reverse faults are also well-developed (Sharp et al., 2000a). These faults dip 10–30° to the NE, have <50 cm displacement and cluster within mudstone-dominated units. Where massive pre-rift carbonates or sandstones occur in the immediate hanging wall to the master fault, closely-spaced joints and fractures are developed that dip moderately ($<40°$) towards the NE and display slickensides which indicate top-to-the-SSW slip (stereonet B; Fig. 4).

6. Style and sequence of deformation during fault-propagation folding

Based on the relationship between the master faults, fault-propagation folds and meso- and macro-scale deformation structures, we propose a model for the style and sequence of deformation during fault-propagation folding (Fig. 13). This model is based on a compilation of key observations from all of the studied fault zones within the study area and we consider this synthesis equally applicable to other extensional settings.

6.1. Fold initiation

During the early stages of fault growth, a monoclinal growth fold developed above the blind fault tip within the mixed carbonate–clastic units of Megasequence Two (Stages A and B; Fig. 13). Based on the observation that basement and Megasequence One are typically faulted and not folded, Sharp et al. (2000a) suggested that faults nucleated at depth within granitic basement and propagated upwards into and caused folding within the overlying mixed carbonate–clastic succession of Megasequences Two and Three. With continued fault-slip and upwards tip propagation, there was net movement of material from the proto-footwall to the proto-hanging wall within the mechanically layered succession, resulting in fault-perpendicular extension of the proto-footwall (Stage B; Fig. 13) (cf. Withjack et al., 1990; Pascoe et al., 1999). Towards the base of the monocline, extension was accommodated at the largest scale by layer-parallel slip along thick, mechanically weak mudstone-dominated units such as the Raha and Duwi Formations (e.g. Stage B; Fig. 13) and macro-scale normal faulting in the stronger carbonate and sandstone lithologies such as the Wata and Sudr Formations (Stage C; Fig. 13). At the smallest scale, extension was accommodated by layer-parallel slip, which also occurred along thin (<1 m) mudstone horizons, with differential movement on superjacent and subjacent slip horizons causing normal faulting and block rotation within 2–10-m-thick carbonate and sandstone-dominated units (see inset Stage C; Fig. 13) (cf. Gross et al., 1997).

In the proto-hanging wall, where the master fault had a planar map-view along-strike trend, a series of fault-parallel, sub-vertical normal faults formed, which were part of a 100–200-m-wide fault zone. However, where the master fault had a pronounced convex-into-the-footwall map-view trace, space problems associated with vertical displacement across an arcuate (concave) normal fault plane occurred. In these locations macro-scale reverse faults began to splay off the master fault and propagate upwards and outwards into the steep

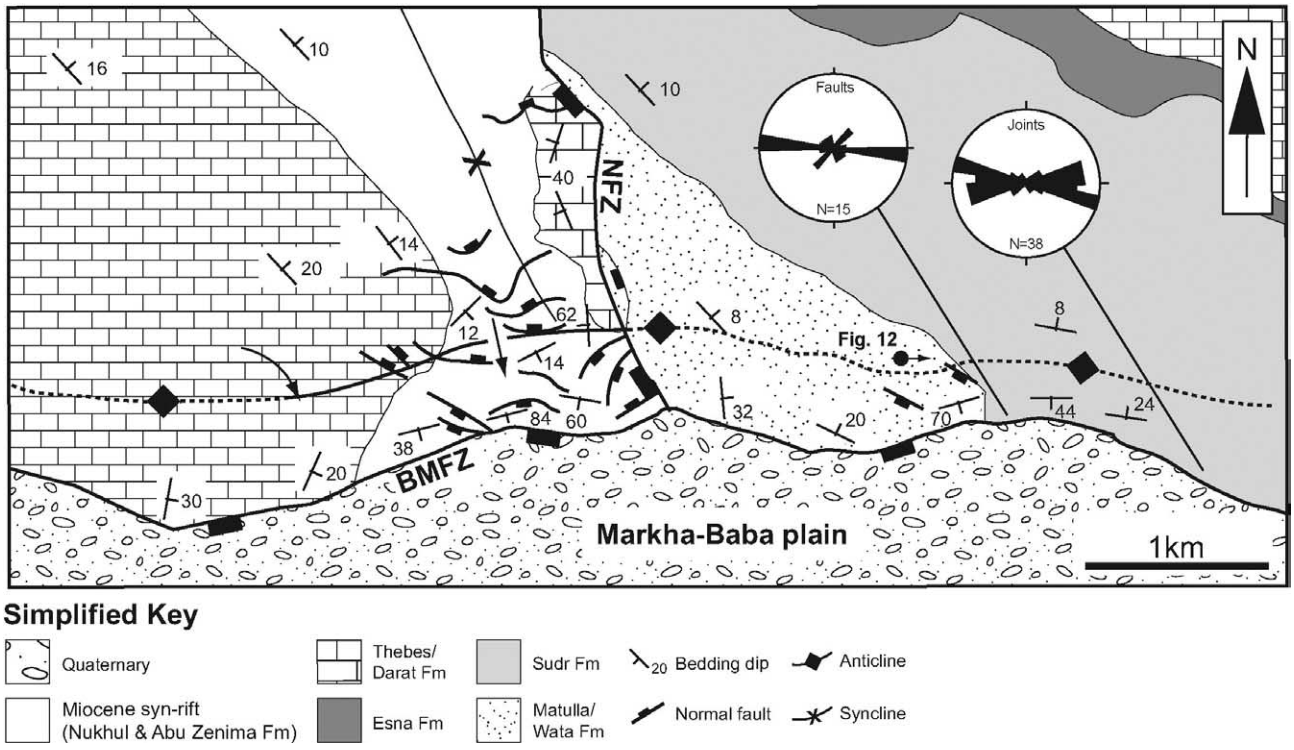

Fig. 11. Simplified geological map of the Baba-Markha fault zone. Note the marked along-strike variability in lithology and meso-scale normal fault development in the footwall to this structure. Rose diagrams are provided for low-displacement (<1 m) faults and joints developed in chalk units of the Sudr Formation. See Fig. 2A for location of map. The location of Fig. 12 is shown.

limb of the hanging wall syncline (Stages B and C; Fig. 13) (cf. Sharp et al., 2000a). As observed in the proto-footwall, marked spatial partitioning in the style of deformation due to lithology occurred in the proto-hanging wall, with low-displacement faulting and folding occurring predominantly within mudstone-dominated units whereas massive carbonate and sandstone-dominated units were pervasively fractured and jointed.

6.2. Fold amplification and breaching

With continued fault slip and tip propagation, normal faults in the immediate hanging wall and above the master fault either became linked and incorporated into the master fault (cf. Fig. 1A) or became inactive (Stage C; Fig. 13). At deeper structural levels within the monocline, continued fault slip led to amplification of the fault-propagation fold and rotation of bedding in the steep limb of the monocline. As bedding within the steep limb of the monocline became rotated towards vertical, rider blocks bound by macro-scale faults immediately adjacent to the master fault were deformed, with mudstone-dominated units becoming sheared and attenuated, and carbonate and sandstone-dominated units being fractured and brecciated. Macro-scale normal faults may have also been passively rotated and overturned to appear as steeply-dipping reverse faults. Meso-scale faults were also affected by progressive rotation of the monocline steep limb, with synthetic and antithetic faults rotating to steeper and shallower dips, respectively, and eventually becoming overturned (Stages C and D; Fig. 13). With time, breaching of layer-parallel slip horizons by the master fault at depth within the fold caused the faults associated with these horizons to become inactive. At higher structural levels above the propagating fault tip, new layer-parallel slip horizons and associated macro- and meso-scale faults began to form as slip was transferred to younger, mechanically weak mudstone-dominated horizons such as the Esna Formation and the heterolithic Nukhul Formation (Stage C; Fig. 13). Based on stratigraphic data from syn-rift depocentres in the footwall to the CFB it is observed that meso- and macro-scale faults in the upper part of the fault-propagation fold were active 3.8 My after the initiation of rifting, thereby pre-dating activity on the CFB by 2.2–3.2 My (based on ages provided by Gawthorpe et al. (2003)) and suggesting they formed while the master fault was still blind and expressed at surface as a monocline (Stages C and D; Fig. 13). A progressive upwards younging of secondary structures is also observed in the proto-hanging wall, with successive reverse faults propagating outward into the hanging wall of the master fault at progressively higher structural levels, causing rotation of older, underlying reverse faults in their footwalls (Stage D; Fig. 13). Macro-scale faults in the proto-footwall of the fault-propagation fold also continued to grow through vertical and lateral propagation of their tips (Stage D; Fig. 13).

With continued slip and upward propagation of the master fault the monocline was breached, growth folding ceased and deformation was localised onto the master fault (Stage E;

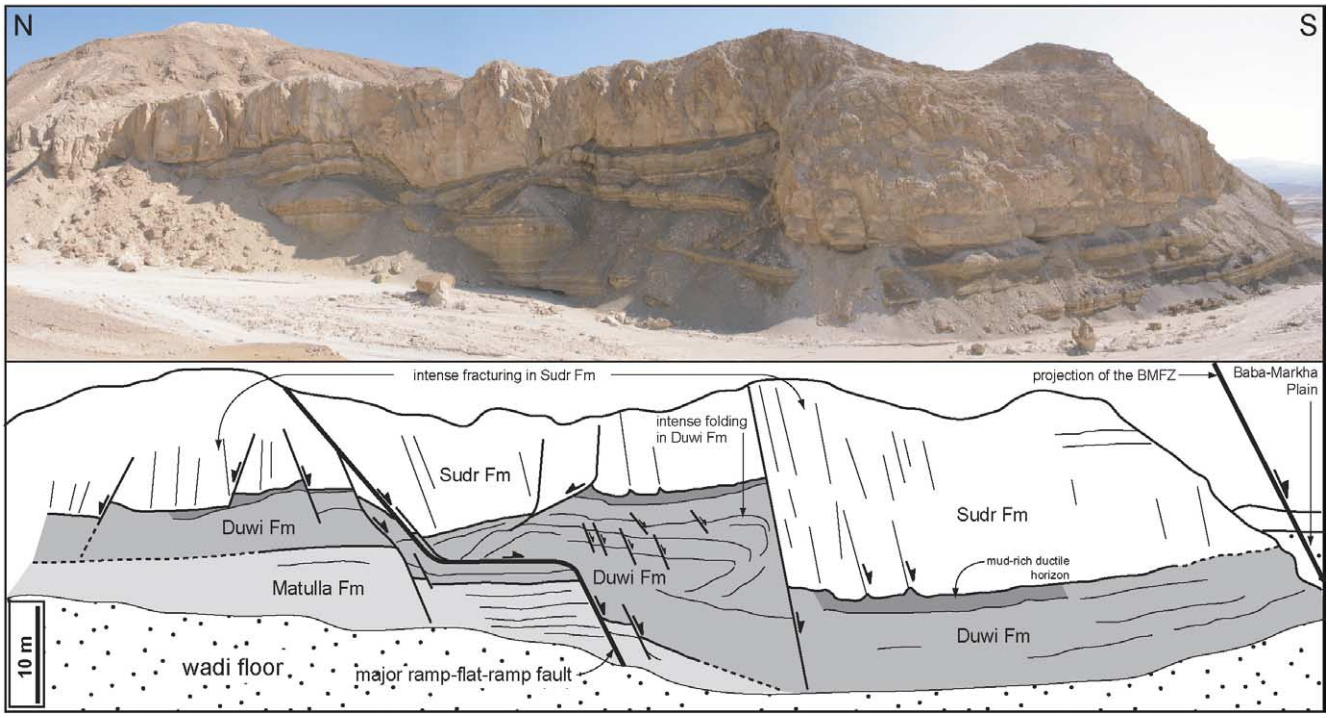

Fig. 12. (A) Field photograph and (B) interpretative line drawing of complex meso-scale faulting in the footwall to the Baba-Markha fault zone. Intense faulting, fracturing and jointing within the carbonate Sudr Formation and sandstone Matulla Formation contrasts with the intense folding and attenuation of mudstone-dominated Duwi Formation. See Fig. 11 for location.

Fig. 13). The master fault eventually became a surface-breaking feature that, with increasing displacement, generated a more typical half-graben style basin in its hanging wall. Continued slip on the master fault was probably still associated with drag of steeply-dipping beds immediate adjacent to the fault zone, causing additional shearing of mudstone units and brecciation of carbonate and sandstone units.

7. Discussion and conclusions

Structural analysis of well-exposed fault zones and associated folds from the Suez Rift has provided important insights into the evolution of fault propagation folds in extensional settings, in particular the manner in which deformation is accommodated during fault propagation folding. In this section some of the key observations from this study are compared and contrasted with predictions made by numerical and physical analogue models and observations from other field examples where fault-propagation folding is observed.

Numerical and physical analogue models have been used to investigate the style and sequence of deformation during extensional fault-propagation folding. Both modelling approaches suggest that fold-related strain is accommodated by small-scale faulting in mechanically strong units and ductile flow, folding and layer-parallel slip in mechanically weak units (e.g. Withjack et al., 1990; Patton and Fletcher, 1995; Cooke and Pollard, 1997; Allmendinger, 1998; Hardy and McClay, 1999; Finch et al., 2004) (e.g. Fig. 1C). The majority of numerical models typically only predict bulk strain distribution through time, however, and thus the structural style and orientation of secondary structures accommodating this strain must be inferred (e.g. Fig. 1C; see Finch et al. (2004) for exception). Although physical analogue models can physically reproduce secondary structures, they are typically constructed on the centimetre-scale (e.g. Fig. 1A), thus are too small to allowed detailed analysis of the style of secondary deformation.

Field data from the Suez Rift confirms many of the bulk deformation characteristics of fault-propagation folds highlighted by numerical and physical analogue models. For example, during the early stages of fault-propagation folding, the proto-footwall is a site of net extension which is accommodated by macro- to meso-scale normal faults in carbonate and sandstone-dominated units and layer-parallel slip within centimetre- to decimetre-thick mudstone-dominated units (cf. Fig. 1B). The proto-hanging wall, where deformation style is also observed to be controlled by lithology, is also a site of net extension although this situation is locally complicated where the map-view trace of the master

slip and faulting to be transferred to shallower horizons. Initiation of macro-scale faulting in the proto-footwall. (D) Continued propagation of the master fault and further amplification of the fault-propagation fold. Vertical and lateral propagation of macro-scale footwall faults. A second reverse fault splays off the master fault into the hanging wall and rotates the underlying structure. (E) Breaching of the fault-propagation fold. Note that meso-scale faults are cross-cut by the master fault.

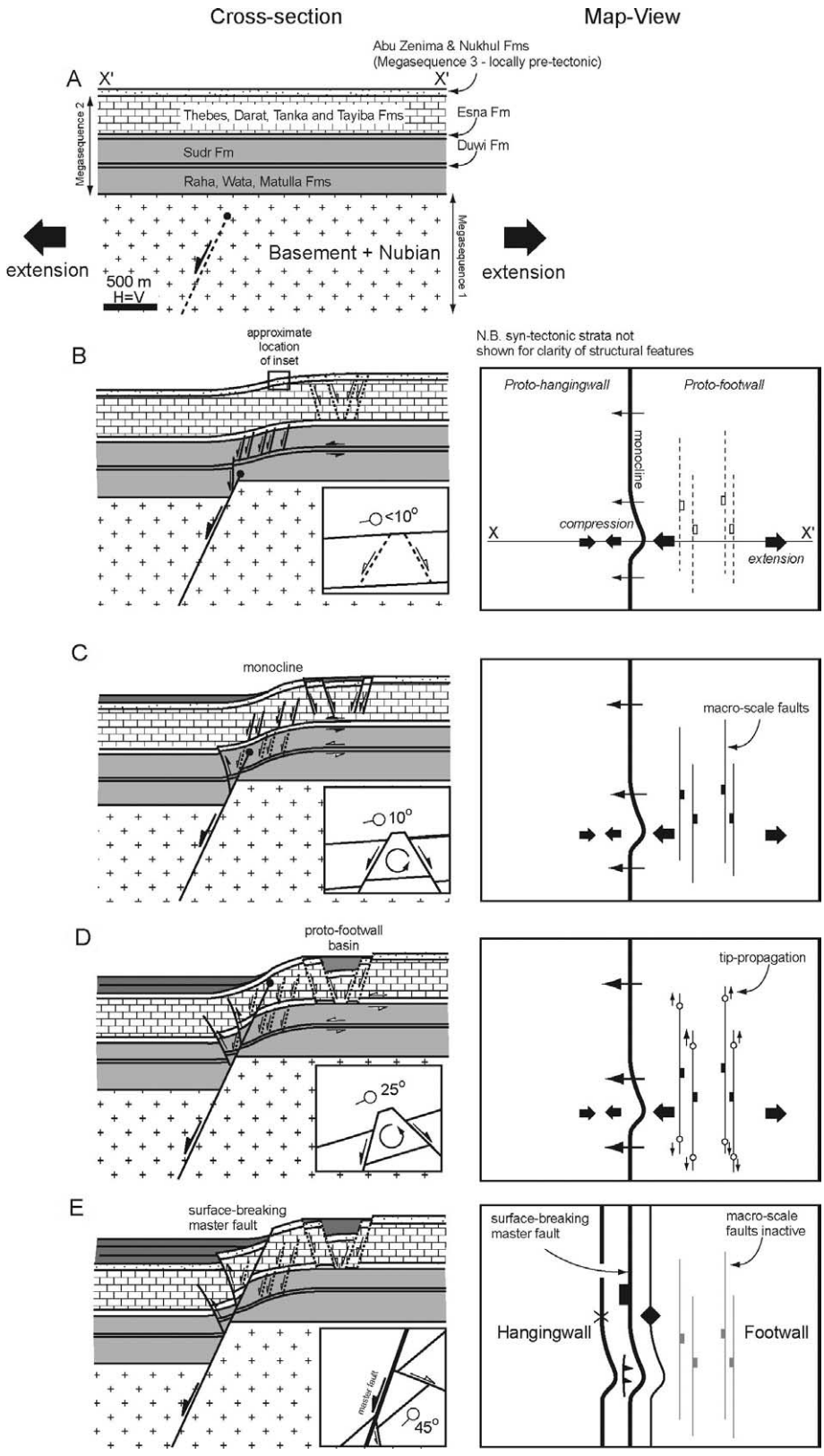

Fig. 13. Cross-sections (X–X′) and corresponding map-view diagrams illustrating the conceptual model for the style and sequence of deformation during fault-propagation folding based on observations from the Suez Rift. Only major layer-parallel slip horizons and faults are shown for clarity. Insets show the evolution of meso-scale structures in the immediate proto-footwall of the fault. (A) Pre-extension. (B) Initiation of master fault propagation at depth and development of a monoclinal growth fold in the cover stratigraphy. Layer-parallel slip occurs along major mudstone-dominated units at depth and carbonate-dominated units deform mainly by faulting Steep-dipping normal faults splay off the master fault into the hanging wall. (C) Continued upward propagation of the master fault and amplification of the fault-propagation fold. Breaching of the lower layer-parallel detachment causes faulting associated with this horizon to cease and layer-parallel

fault is not planar (see below). A lithological control on deformation style and magnitude similar to that observed in modelling studies has also been documented in field studies by Gross et al. (1997) from the western margin of the Dead Sea Rift, southern Israel, and by Fodor et al. (2005) from the Sirt Basin, south-central Libya. In these settings, layer-parallel slip and ductile flow occur in mechanically weak mudstone units whereas carbonate and sandstone units are faulted and fractured.

Although results from the Suez Rift compare favourably with predictions made by numerical and physical analogue models, this study also highlights several important controls on the evolution of fault-propagation folds that are not captured by these models. For example, numerical modelling studies that have investigated the influence of cover stratigraphy strength on the style and magnitude of deformation during fault-propagation folding either indirectly by using the propagation-to-slip ratio of the propagating fault as a proxy for cover stratigraphy strength (e.g. Hardy and McClay, 1999) or by directly modelling a mechanically-layered cover stratigraphy of varying strength (Finch et al., 2004), have only considered vertical (stratigraphic) changes in lithology. Our results, although confirming that the mechanical strength of the cover stratigraphy is a prominent control on the structural style and heterogeneity of secondary deformation associated with fault-propagation, also indicate that lateral, along-strike lithological variations at any one structural level within an evolving fault-related fold may also result in marked lateral heterogeneity in deformation mechanisms, which in turn results in a complex spatial organisation of structures. Such along-strike variations in deformation style due to lithological heterogeneity are well illustrated in the footwall of the Baba-Markha fault zone (e.g. Fig. 11). Secondly, our field data indicates that reverse faults and associated folds may be locally well-developed where the master fault has a convex-into-the-footwall map-view trace. In contrast, in numerical and physical analogue models, reverse faults are only rarely observed and are subordinate compared with extensional structures. The observation that the magnitude of hanging wall compression and reverse faulting is closely-related to the map-view geometry of the master fault suggests that existing 2D numerical and physical analogue models, which only consider variations in fault orientation with depth (e.g. dip) and not laterally along-strike, may be underestimating the importance of macro-scale hanging wall reverse faulting during fault-propagation folding.

Another aspect of fault-propagation folding not captured by existing models is the temporal evolution of secondary structures accommodating strain. For example, our data indicates that secondary structures adjacent to the master faults are not all active at the same time and may initiate and die at different stages during the evolution of the fault-propagation fold. For example, as the fault-tip propagates through the cover, layer-parallel slip horizons are dissected and become inactive, as do the faults associated with them. Simultaneously, however, layer-parallel slip horizons and normal faults associated with them are initiated within overlying mechanically weak horizons within the evolving fold and are active until they too are breached by the master fault. Normal and reverse macro-scale faults also display a similar dynamic behaviour, propagating laterally and vertically through time in response to increasing displacement on the master fault. Such observations are not immediately apparent from numerical and physical analogue models due to: (1) the inability of the models to directly model secondary structures (e.g. Fig. 1C), (2) the models being too small to allow detailed observation of secondary structures (e.g. Fig. 1A), and/or (3) the models being 2D, thus limiting observation of deformation patterns above the propagating fault at the free-surface (Fig. 1A–C).

Acknowledgements

This study was supported by the Natural Environment Research Council (Studentship GT04/98/197/ES to CALJ and Research Grant GR3/12947 to RLG). Thanks to Roy Schlische, an anonymous referee and Cath Hunt for comments that helped to improve considerably the clarity of this manuscript. Thanks also to Michael Young, Ian Carr and David Pivnik for discussions in the field. Sayeed and Gamal Gouda are also thanked for excellent field lunches and logistical support. This paper is dedicated to Andrew Jackson.

References

Allmendinger, R.W., 1998. Inverse and forward numerical modelling of trishear fault-propagation folds. Tectonics 17, 62–81.

Bentham, P.A., Wescott, W.A., Krebs, W.H., Lund, S.P., 1996. Magnetostratigraphic correlation and dating of the early to middle Miocene stratigraphy within the Suez Rift. American Association of Petroleum Geologists 79, 1197–1198.

Carr, I.D., Gawthorpe, R.L., Jackson, C.A.L., Sharp, I.R., Sadek, A., 2003. Sedimentology and sequence stratigraphy of early syn-rift tidal sediments: the Nukhul Formation, Suez Rift, Egypt. Journal of Sedimentary Research 73, 407–420.

Colletta, B., Moretti, I., 1985. Structural analysis in the Wadi Baba area. Institut Francais du Petrole (IFP) Report 27401.

Colletta, B., Le Quellec, P., Letouzy, J., Moretti, I., 1988. Longitudinal evolution of the Suez Rift structure (Egypt). Tectonophysics 153, 221–233.

Cooke, M.L., Pollard, D.D., 1997. Bedding-plane slip in initial stages of fault-related folding. Journal of Structural Geology 19, 567–581.

Corfield, S.C., Sharp, I.R., 2000. Structural style and stratigraphic architecture of fault propagation folding in extensional settings: a seismic example from the Smørbukk area, Halten Terrace, Mid-Norway. Basin Research 12, 329–341.

Erslev, E.A., 1991. Trishear fault-propagation folding. Geology 19, 617–620.

Finch, E., Hardy, S., Gawthorpe, R.L., 2004. Discrete-element modelling of extensional fault-propagation folding above rigid basement fault blocks. Basin Research 16, 467–488.

Fodor, L., Turki, S.M., Dalub, H., Al Gerbi, A., 2005. Fault-related folds and along-strike dip segmentation of breaching faults: syn-diagenetic deformation in the south-western Sirt basin, Libya. Terra Nova 17, 121–128.

Garfunkel, Z., Bartov, Y., 1977. Tectonics of the Suez Rift. Geological Survey of Israel Bulletin 71, 1–41.

Gawthorpe, R.L., Sharp, I.R., Underhill, J.R., Gupta, S., 1997. Linked sequence stratigraphic and structural evolution of propagating normal faults. Geology 25, 795–798.

Gawthorpe, R.L., Jackson, C.A.L., Young, M.J., Sharp, I.R., Moustafa, A.R., Leppard, C.W., 2003. Normal fault growth, displacement localisation and the evolution of normal fault populations: the Hammam Faraun fault block, Suez Rift, Egypt. Journal of Structural Geology 25, 883–895.

Gilpin, R., 1998. Controls on structural geometries and sediment dispersal in dissected relay ramps: evolution of the Baba fault, eastern Gulf of Suez. Unpublished MRes thesis, University of Edinburgh.

Grant, J.V., Kattenhorn, S.A., 2004. Evolution of vertical faults at an extensional plate boundary, southwest Iceland. Journal of Structural Geology 26, 537–557.

Gross, M.R., Becker, A., Gutiérrez-Alonso, G., 1997. Transfer of displacement from multiple slip zones to a major detachment in an extensional regime: examples from the Dead Sea rift, Israel. Geological Society of American Bulletin 109, 1021–1035.

Gupta, S., Underhill, J.R., Sharp, I.R., Gawthorpe, R.L., 1999. Role of fault interactions in controlling syn-rift sediment dispersal patterns: Miocene, Abu Alaqa Group, Suez Rift, Sinai, Egypt. Basin Research 11, 167–189.

Hardy, S., McClay, K., 1999. Kinematic modelling of extensional fault-propagation folding. Journal of Structural Geology 21, 695–702.

Jackson, C.A.L., Gawthorpe, R.L., Sharp, I.R., 2002. Growth and linkage of the East Tanka fault zone; structural style and syn-rift stratigraphic response. Journal of the Geological Society of London 159, 175–187.

Jackson, C.A.L., Gawthorpe, R.L., Leppard, C.W., Sharp, I.R., 2006. Rift-initiation development of normal fault blocks: insights from the Hammam Faraun fault zone block, Suez Rift, Egypt. Journal of the Geological Society of London 163, 165–183.

Janecke, S.U., Vanderburg, C.J., Blankenau, J.J., 1998. Geometry, mechanism, and significance of extensional folds from examples in the Rocky Mountain Basin and Range province, U.S.A. Journal of Structural Geology 20, 841–856.

Keller, J.V.A., Lynch, G., 2000. Displacement transfer and forced folding in the Maritimes basin of Nova Scotia, eastern Canada. In: Cosgrove, J.W., Ameen, M.S. (Eds.), Forced Folds and Fractures Geological Society of London Special Publication 169, pp. 87–101.

Khalil, S.M., McClay, K.R., 2002. Extensional fault-related folding, north-western Red Sea, Egypt. Journal of Structural Geology 24, 743–762.

Knott, S.D., 2001. Gravity-driven crustal shortening in failed rifts. Journal of the Geological Society of London 158, 193–196.

Knott, S.D., Beach, A., Welbon, A.L., Brockbank, P.J., 1995. Basin inversion in the Gulf of Suez: implications for exploration and development in failed rifts. In: Buchanan, J.G., Buchanan, P.G. (Eds.), Basin Inversion Geological Society of London Special Publication, 88, pp. 59–81.

Krebs, W.N., Wescott, W.A., Nummedal, D., Gaafar, I., Azazi, G., Karamat, S., 1997. Graphic correlation and sequence stratigraphy of Neogene rocks in the Gulf of Suez. Bulletin of the Geological Society of France 168, 63–71.

Lyberis, N., 1988. Tectonic evolution of the Gulf of Suez and the Gulf of Aqaba. Tectonophysics 153, 209–220.

Maurin, J.-C., Niviere, B., 2000. Extensional forced folding and décollement of the pre-rift series along the Rhine Graben and their influence on the geometry of the syn-rift sequences. In: Cosgrove, J.W., Ameen, M.S. (Eds.), Forced Folds and Fractures Geological Society of London Special Publication 169, pp. 73–86.

Mitra, S., Islam, Q.T., 1994. Physical (clay) models of inversion structures. Tectonophysics 230, 211–222.

Montenat, C., Orszag-Sperber, F., Plaziat, J.C., Purser, B.H., 1998. The sedimentary record of the initial stages of Oligo-Miocene rifting in the Gulf of Suez and the northern Red Sea. In: Puser, B.H., Boscence, D.W.J. (Eds.), Sedimentation and Tectonics in Rift Basins; Red Sea–Gulf of Aden Chapman & Hall, London, pp. 146–164.

Moustafa, A.R., 1987. Drape folding in the Baba-Sidri area, eastern side of the Suez Rift, Egypt. Journal of Geology 31, 15–27.

Moustafa, A.R., 1993. Structural characteristics and tectonic evolution of the east-margin blocks of the Suez Rift. Tectonophysics 223, 381–399.

Moustafa, A.R., Abdeen, A.R., 1992. Structural setting of the Hammam Faraun fault block, eastern side of the Suez Rift. Journal of the University of Kuweit (Science) 19, 291–310.

Pascoe, R., Hooper, R., Storhaug, K., Harper, H., 1999. Evolution of extensional styles at the southern termination of the Nordland Ridge, mid-Norway: a response to variations in coupling above Triassic salt. In: Fleet, A.J., Boldy, S.A.R. (Eds.), Petroleum Geology of Northwest Europe Proceedings of the 5th Conference, pp. 83–90.

Patton, T.L., 1984. Normal faulting and fold development in sedimentary rocks above a pre-existing basement normal fault. Unpublished PhD thesis, Texas A and M University.

Patton, T.L., 2004. Numerical models of growth-sediment development above an active monocline. Basin Research 16, 25–39.

Patton, T.L., Fletcher, R.C., 1995. Mathematical block-motion model for deformation of a layer above a buried fault of arbitrary dip and sense of slip. Journal of Structural Geology 17, 1455–1472.

Patton, T.L., Moustafa, A.R., Nelson, R.A., Abdine, S.A., 1994. Tectonic evolution and structural setting of the Suez Rift. In: Landon, S.M. (Ed.), Interior Rift Basin American Association of Petroleum Geologists Memoir 59, pp. 7–55.

Robson, D.A., 1971. The structure of the Gulf of Suez (Clysmic) rift, with special reference to the eastern side. Journal of the Geological Society of London 127, 247–276.

Schlische, R.W., 1995. Geometry and origin of fault-related folds in extensional settings. American Association of Petroleum Geologists Bulletin 79, 1661–1678.

Sharp, I.R., Gawthorpe, R.L., Underhill, J.R., Gupta, S., 2000a. Fault propagation folding in extensional settings: examples of structural style and syn-rift sedimentary response from the Suez Rift, Egypt. Geological Society of America Bulletin 112, 1877–1899.

Sharp, I.R., Gawthorpe, R.L., Armstrong, B., Underhill, J.R., 2000b. Propagation history and passive rotation of mesoscale normal faults: implications for syn-rift stratigraphic development. Basin Research 12, 285–306.

Sterns, A.R., 1978. Faulting and forced folding in the Rocky Mountains foreland. In: Matthews, V. (Ed.), Laramide Folding Associated with Basement Block Faulting in the Western United States Geological Society of America Memoir 151, pp. 1–37.

Vendeville, B., 1987. Champs de failles et tectonique en extension: modelesiation physicale. PhD Thesis, Universite de Rennes, Rennes, France, 395pp.

Willsey, S.P., Umhoefer, P.J., Hilley, G.E., 2002. Early evolution of an extensional monocline by a propagating normal fault: 3D analysis from combined filed study and numerical modelling. Journal of Structural Geology 24, 651–669.

Withjack, M.O., Callaway, S., 2000. Active normal faulting beneath a salt-layer: physical study of deformation patterns in the cover sequence. American Association of Petroleum Geologists Bulletin 84, 627–651.

Withjack, M.O., Meisling, K.E., Russell, L.R., 1989. Forced folding and basement-detached normal faulting in the Haltenbanken area, offshore Norway. In: Tankard, A.J., Balkwill, H.R. (Eds.), Extensional Tectonics and Stratigraphy of the North Atlantic Margins American Association of Petroleum Geologists Memoir 46, pp. 567–575.

Withjack, M.O., Olson, J., Peterson, E., 1990. Physical models of extensional forced folds. American Association of Petroleum Geologists Bulletin 74, 1038–1054.

Young, M.J., Gawthorpe, R.L., Sharp, I.R., 2002. Architecture and evolution of syn-rift clastic depositional systems towards the tip of a major fault segment, Suez Rift, Egypt. Basin Research 14, 1–23.